doi: 10.56761/EFRE2022.N1-O-038602

Dynamic fracture of hexagonal close packed alloys

V.V. Skripnyak[*]*, E.G. Skripnyak, V.A. Skripnyak*

National Research Tomsk State University, Tomsk, Russia
[*]*skrp2012@yandex.ru*

Abstract. The paper presents the results of 3D numerical simulation of the processes of deformation and ductile fracture of hexagonal close packed titanium and zirconium alloys under dynamic impacts. Based on the generalization of the obtained experimental data, a version of the model is proposed that allows to adequately describe the regularities of plastic deformation during tension, the formation of zones of localization of plastic shears and the development of damage and fracture in a wide range of strain rates and spall fracture in plates under plane shock waves impacts. Proposed constitutive equation described the mechanical response of HCP titanium and zirconium alloys in a wide range of strain rates at the temperatures below temperature of phase transformation. It was shown that using of the kinetic model of the damaged medium is justified at high strain rates in complex stress conditions in the spall zone and around it.

1. Introduction

The need to predict the mechanical behavior of metals and alloys with a hexagonal close-packed (HCP) lattice under dynamic loads arises when solving a wide range of applied problems. HCP metals and alloys are being used in critical structures of energetic equipment and transport systems due to their high specific strength properties in comparison with traditional face-centered cubic (FCC) and the body centered cubic (BCC) alloys [1, 2]. A number of constitutive equations and fracture models of HCP alloys have been proposed [3–6]. Zerilli and Armstrong proposed constitutive models based on the dislocation kinetics of plastic flow and taking into account the difference in the regularities of strain hardening, thermal softening, and flow stress rate sensitivity for FCC and BCC metals with face-centered cubic (FCC) lattice, lattice and HCP crystalline lattice [3]. Gao et al. developed a constitutive model for HCP metals, which made it possible to more adequately describe the mechanical behavior of Ti-6Al-4V in a wide range of strain rates and temperatures, in comparison with the constitutive equations of the Johnson-Cook and Armstrong Zerilli models [4]. Nemat-Nasser et al. showed that, in order to adequately describe the high rate deformation of CP-Ti, it is necessary to take into account, in addition to the motion of dislocations, the contributions of twins [5]. Song et al analyzed the experimental data of Nemat-Nasser and proposed a model to describe the influence of the dynamic strain aging on the mechanical behavior of titanium alloys in a wide range of strain rates and temperatures up to 1000 K [6]. At the same time, the question of the adequacy of the proposed models for describing the mechanical response of various HCP metals and alloys under dynamic loading remained open.

Frost et al. showed the similarity laws of the mechanical behavior of HCP alloys subgroups in the temperature range of crystal lattice stability and a wide range of strain rates [7]. The unit cell of HCP crystalline lattice can be imagined as a hexagonal prism with one atom on each vertex, and 3 atoms in the center. In contrast to cubic unit cells of FCC and BCC crystals, HCP unit cell has two different crystal lattice parameters c and a ($c > a$).

HCP alloys can be divided into three isomechanical subgroups, depending on the ratio of the crystal lattice parameters (c/a), where c and a are parameter of crystalline cell [8]. The first subgroup includes HCP metals (α-Ti, α-Zr, Hf, α-Be, Sc, Y, Ru) has the ratio c/a <1.633, the second subgroup includes Mg, and Co has the ratio $c/a \approx 1.623$, and the third subgroup includes metals Zn, Cd, La, Pr with c/a> 1.633 [7].

This work aimed to study the processes of deformation, damage and ductile fracture of HCP alloys under dynamic influences. Based on the generalization of the obtained experimental data, a version of the model is proposed that allows to adequately describe the regularities of plastic

deformation during tension, the formation of zones of localization of plastic shears and the development of damage and fracture in the range of strain rates from 10^{-3} to 10^{3} s^{-1} at the values of the triaxiality parameter of the stress state from 0.33 to 0.6 [1, 2]. The model was used for 3D numerical modeling of uniaxial tension of specimens and spall fracture in Ti, Zr plates under plane shock waves impacts. The influence of the damage parameter, the stress state triaxiality parameter on the flow stress is taken into constitutive equation.

2. **Numerical simulation of plastic flow and damage evolution**

The response of HCP alloys to dynamic influences in a wide temperature range was described by a model of a damaged elastic viscoplastic medium [9]. The system of equations according the Lagrangian approach includes conservation equations of isotropic continual medium (1), kinematic relations (2), constitutive relations (7), Birch – Murnaghan equation of state of HCP phase of titanium and zirconium alloys (4) [10, 11], relaxation equation for the deviatoric stress tensor (5), plastic potential (6), thermodynamic relations (7)–(8), equations describing the dependence of elastic modulus temperatures and pressure (9).

$$d\rho / dt = \rho \partial u_i / \partial x_i, \quad d\rho/dt = \rho \partial u_i/\partial x_i, \ \partial \sigma_{ij}/\partial x_j = \rho \, du_i/dt, \ \rho(dE)/d\,t = \sigma_{ij}\dot{\varepsilon}_{ij}, \tag{1}$$

$$\dot{\varepsilon}_{ij} = (1/2)\left(\partial u_i/\partial x_j + \partial u_j/\partial x_i\right), \ \dot{\omega}_{ij} = (1/2)\left(\partial u_i/\partial x_j - \partial u_j/\partial x_i\right), \tag{2}$$

$$\sigma_{ij} = -p\delta_{ij} + S_{ij}, \tag{3}$$

$$\begin{cases} p = p^{(m)}\,\Psi_1(f),\ S_{ij} = S_{ij}^{(m)}\Psi_2(f), \\ p^{(m)} = p_x^{(m)}(\rho) + \Gamma(\rho)\rho E_T, \\ E = E_c + E_T, \\ p_x^{(m)} = 3B_0 \cdot (\rho_0/\rho)^{-2/3} \cdot \left(1-(\rho_0/\rho)^{1/3}\right) \cdot \exp\left[\frac{3}{2}(B_1-1)\cdot\left(1-(\rho_0/\rho)^{1/3}\right)\right] if\ p^{(m)} \ge 0, \\ p_x^{(m)} = B_0(1-\rho_0/\rho)\ if\ \ p^{(m)} < 0, \\ E_{\mathrm{T}} = C_p^{(m)}T, \end{cases} \tag{4}$$

$$\begin{cases} DS_{ij}^{(m)}/Dt = 2\mu\left(\dot{\varepsilon}_{ij}^{e} - \delta_{ij}\dot{\varepsilon}_{kk}^{e}/3\right), \\ DS_{ij}^{(m)}/Dt = dS_{ij}^{(m)}/dt - S_{ik}^{(m)}\dot{\omega}_{jk} - S_{jk}^{(m)}\dot{\omega}_{ik}, \\ \dot{\varepsilon}_{ij} = \dot{\varepsilon}_{ij}^{e} + \dot{\varepsilon}_{ij}^{p},\ \dot{\varepsilon}_{ij}^{p} = \dot{e}_{ij}^{p} + \delta_{ij}\dot{\varepsilon}_{kk}^{p}/3, \\ \dot{e}_{ij}^{p} = \lambda\partial\Phi/\partial\sigma_{ij}, \\ \dot{\varepsilon}_{kk}^{p} = \dot{f}_{growth}/(1-f). \end{cases} \tag{5}$$

$$\Phi = \left(\sigma_{eq}{}^2/\,\sigma_s{}^2\right) + 2q_1 f^* \cosh\left(-q_2\, p/2\sigma_s\right) - 1 - q_3\left(f^*\right)^2, \tag{6}$$

where ρ is the mass density, u_i is the components of the particle velocity vector, x_i is Cartesian coordinates, I = 1, 2, 3, E is the specific internal energy, $\dot{\varepsilon}_{ij}, \dot{\omega}_{ij}$, are the components of strain rate

tensor and the bending–torsion tensor, the $\psi_i(f)$ functions established a relation between the effective stresses of the damaged medium and the stresses in the condensed phase, Γ is the Grüneisen coefficient, ρ_0 is the initial mass density of the condensed phase of the alloy, γ_R, ρ_R, n, B_0, B_1 are the material's constants, C_p is the specific heat capacity, $D(\cdot)/Dt$ is the Jaumann's derivative, μ is the shear modulus, $\dot{f}_{growth}$ is the void growth rate, f is the damage parameter, σ_s is the yield stress, σ_{eq} is equivalent stress, p is the pressure, q_1, q_2, and q_3 are model parameters, and f_* is the specific volume of damages λ is the plastic multiplier derived from the consistency condition $\Phi = 0$, and Φ is the plastic potential.

Parameters of HCP titanium and zirconium equation of state are shown in Table 1.

Table 1. Parameters of HCP titanium and zirconium

At. Number/ Symbol	Metals	*c/a*	ρ_0, (g/cm^3)	μ (GPa) at 295 K	ν	B_0 (GPa)	B_0'	T_m (K)	T_{pt} (K)	Isomechanical subgroup
22 Ti	α-Titanium	1.58734	4.51	42.65	0.327	108.9	4.4	1941	1155	I
40 Zr	α-Zirconium	1.59312	6.49	36.17	0.336	98.4	3.8	2128	1135	I

For the HCP titanium and zirconium alloys the Grüneisen parameter was assumed equal to $\Gamma = 1.09$.

The criterion of plasticity (6) for damaged media proposed by Gurson and modified by Tvergaard was used for dynamic loadings simulation of HCP alloys [12–14]. The dynamic yield stress Y_{HEL} (T) at the Hugoniot elastic limit can be determined by formula (7) taking into account (8).

$$Y_{HEL} = \frac{(1-\nu)}{(1+2\nu)}\sigma_{HEL}. \tag{7}$$

The Hugoniot elastic limit σ_{HEL} (T) of shock-loaded alloys at the initial temperature T can be estimated by relation (8) taking into account C_L (T) and ρ (T) [9]:

$$\sigma_{HEL}(T)=\rho(T)C_L(T)u_{HEL,} \tag{8}$$

where u_{HEL} is amplitude of the particles velocity in the elastic precursor, C_L is longitudinal sound velocity.

The model constitutive equation of the considered isomechanical subgroup of HCP alloys takes into account the effect on the flow stress of the temperature T, the equivalent strain rate, accumulated equivalent plastic strain, the pressure p, and the overage grain size d_g.

$$\sigma_s = \sigma_s\left(\varepsilon_{eq}^p, T, \dot{\varepsilon}_{eq}^p, p, d_g\right). \tag{9}$$

Unlike FCC and BCC metals and alloys, plastic deformation of single crystals and grains of metals with an HCP lattice is caused not only by the sliding of dislocations along prismatic, pyramidal and basic systems with significantly different Burgers vectors, but also by twinning in a number of systems.

It is proposed to represent the macroscopic plastic flow stress as the sum of the contributions of the stresses required to overcome the resistance to dislocation slip, resistance to twinning, and stresses from the inhomogeneity of the phase composition of the alloy.

$$\sigma_S = \sigma_0 \frac{\mu(T,\rho)}{\mu(295\,K,\rho_0)} + \sigma_s^{disl} + \sigma_s^{tw}, \tag{10}$$

where σ_0 is material parameter depending on the phase composition of the material, $\mu(T, \rho)$ is the shear modulus, ρ_0 is the initial mass density, p is the pressure, σ_s^{disl} is the contribution of dislocation slip to macroscopic flow stress, σ_s^{tw} is the twinning contribution to macroscopic flow stress.
It was proposed to determine the stresses required to ensure dislocation slip in the subgroup of HCP alloys with a ratio of crystal lattice parameters with / a <1.633 using formula (11).

$$\sigma_s^{disl} = \left(C_0\left(\varepsilon_{eq}^p\right)^{1/2} + k_{hp}^{disl} d_g^{-1/2}\right)\exp\left(-\alpha_0 T\right)\exp\left(\alpha_1 T \ln\left(1+\frac{\dot{\varepsilon}_{eq}^p}{\dot{\varepsilon}_{disl0}^p}\right)\right), \tag{11}$$

where d_g is the grain size, k_{hp}^{disl} , C_0, α_0, α_1 are material parameters, $\dot{\varepsilon}_0^p$ is parameter normalizing the plastic strain rate, ε_{eq}^p is the equivalent plastic strain.

The stresses required to ensure twinning σ_s^{tw} were calculated by Eq. (12).

$$\begin{cases} \sigma_s^{tw} = \left(A_0\varepsilon_{eq}^p + k_{hp}^{tw} d_g^{-1/2}\right)\exp\left(-\beta_0 T\right)\exp\left(\beta_1 T \ln\left(1+\frac{\dot{\varepsilon}_{eq}^p}{\dot{\varepsilon}_{tw0}^p}\right)\right)\exp\left(-(2\pi)^{1/2}|N|\right), \\ A_0(\sigma_1 \ge 0) \ne A_0(\sigma_1 < 0), \end{cases} \tag{12}$$

where d_g is the grain size, k_{hp}^{tw}, A_0, β_0, β_1 are material parameters, N is a phenomenological parameter that takes into account the possibility of de twinning when the shear stress sign changes.

Effect of twinning and de-twinning take place in Ti and Zr during loading and unloading.

$$\begin{cases} N = \sum_k \Delta N_k \ , \\ \Delta N_k = \mathrm{sgn}(S_2)\dfrac{\Delta\varepsilon^p{}_k}{n_1\exp\left(-n_2\ln\left(\dfrac{\dot{\varepsilon}_{eq}^p}{\dot{\varepsilon}_0^p}\right)\right)}\dfrac{\mu(T,\rho)}{\mu(295\,K,\rho_0)}\exp\left[(2\pi)^{1/2}\cdot\min\left\{\mathrm{sgn}(-S_2)\cdot N, 0\right\}\right], \end{cases} \tag{13}$$

where S_2 is the second principal stress, n_1, n_2 are constant of material, $\Delta\varepsilon_k^p$ is the increment of equivalent plastic strain during unloading.

Parameters of constitutive equation for some HCP titanium and zirconium alloys are shown in Table 2.

Table 2. Parameters of constitutive equation for several HCP alloys

Alloy	C_0, GPa	k_{hp}^{disl}, GPa $\mu m^{1/2}$	α_0, K^{-1}	α_1, K^{-1}	$\dot{\varepsilon}_{disl0}^p$, s^{-1}	A_0, GPa	k_{hp}^{tw}, GPa $\mu m^{1/2}$	β_0, K^{-1}	β_1, K^{-1}	$\dot{\varepsilon}_{tw0}^p$, s^{-1}
CP Ti	0.4	0.269	0.00224	0.00275	10^3	1.85	0.18	0.0002	0.000973	10^3
Ti-6Al-4V	1.05	0. 269	0.0022	0.00205	10^3	1.85	0.4297	0.0002	0.001809	10^3
Ti-5Al-2.5Sn	0.665	0.628	0.0224	0.002	10^3	1. 5	0.628	0.0002	0.00222	10^3
Zr	1.08	0.250	0.00807	0.000395	10^3	1.03	0.250	0.0001	0.000064	10^3
Zr-1%Nb (E110)	1.68	0.368	0.00807	0.0014	10^3	0.72	0.368	0.0001	0.000064	10^3
Zr-2.5Nb (E625)	1.185	0.368	0.00807-0.00045	0.000395	10^3	0.525	0.368	0.0001	0.000275	10^3

Ductile fracture of HCP alloys is the result of the damage nucleation and growth at the mesoscopic level. The damage nucleation in HCP alloys under dynamic loadings occurs due to the exhaustion of the possibility of local accommodation of plastic deformation in the bands of localized shear or in the zone from the intersection.

Equations (14) were used for describing the kinetics of damage [12, 15].

$$\begin{cases} \dot{f} = \dot{f}_{nucl} + \dot{f}_{growth}; \\ \dot{f}_{growth} = (1-f)\dot{\varepsilon}^{p}_{kk}. \\ \dot{f}_{nucl} = \dot{f}^{(strain)}_{nucl} + \dot{f}^{(stress)}_{nucl}\ ; \\ \dot{f}^{(strain)}_{nucl} = [f_N / (s_N\sqrt{2\pi})]\exp\{-0.5[(\varepsilon^{p}_{eq} - \varepsilon_N)/s_N]^2\}, \\ \dot{f}^{(stress)}_{nucl} = \dot{f}^{(stress)}_{nucl_1} + \dot{f}^{(stress)}_{nucl_2} \\ \dot{f}^{(stress)}_{nucl1} = C_1\dot{\sigma}_{eq} + C_2\dot{\sigma}_{kk} \ \ if \ \ \sigma_{kk} > 0 \ (tension\ in\ the\ spall\ zone); \\ \dot{f}^{(stress)}_{nucl2} = \left[1/\left(\gamma_1 \cdot A_{sn} \cdot \sqrt{2\pi}\right)\right] \cdot \exp\left\{-\left(\ln\left(A_{sn}\right)/\gamma_1 \cdot \sqrt{2}\right)^2\right\}, \\ A_{sn} = \int_0^t \frac{W^e}{\beta_{1sn}\exp\left(-\beta_{2sn}W^p\right)\cdot(1-f)}\frac{dW^p}{dt}dt, \end{cases} \tag{14}$$

where f is the damage parameter, $\dot{f}^{(stress)}_{nucl1}$ is the constituent of $\dot{f}^{(stress)}_{nucl}$ associated with damages caused by negative pressure, $\dot{f}^{(stress)}_{nucl2}$ is the constituent of damages caused by voids evolution under repeated loading, C_1, C_2, f_N, β_{1sn}, β_{2sn}, γ_1 are model parameters, ε_N is the average nucleation strain, s_N is the standard deviation respectively, W_e, and W_p are the specific internal energy, and the specific dissipated energy, respectively.

The modification damage equation (14) makes it possible to describe the kinetics of the damage parameter $\dot{f}^{(stress)}_{nucl}$ increasing at spall fracture as a result of nucleation, growth and coalescence of voids. The specific volume of damages f^* was calculated by relation (15).

$$f^* = f \cdot H(f_c - f) + [f_c + (\overline{f}_F - f_c)/(f_F - f_c)] \cdot H(f - f_c), \tag{15}$$

where f is damage parameter, $H(.)$ is the Heaviside function, $\overline{f}_F = (q_1 + (q_1^2 - q_3)^{1/2})/q_3$, f_c is failure parameter.

Parameters of Eq. (14) and Eq. (15) are shown in Table 3.

Table 3. Dimensionless parameters of the damage model.

Material	q_1	q_2	q_3	f_0	f_N	fc	f_F	ε_N	s_N
CP Ti	1.5	1	1.6	0.001	0.002	0.035	0.12	0.3	0.005
Ti-5Al-2.5Sn	1.	0.7	1.	0 .003	0.1156	0.117	0.260	0.11	0.005
Ti-6Al-4V	1.5	1	1.5	0.001	0.04	0.03	0.04	0.05	0.1
Zr	1.5	1	1	0.001	0.2	0.035	0.4	0.28	0.1
Zr-1% Nb	1.3	1.0	1.69	0.001	0.2	0.035	0.4	0.28	0.1
Zr-2.5% Nb	1.5	1	2.25	0.001	0.004	0.17	0.2	0.3	0.1

The final stage in ductile fracture comprises the voids coalescence. This causes softening of the material and accelerated growth rate of the void fraction f^*. The volume of the material is considered fractured when the percolation threshold of voids is reached in the damaged material.

Macroscopic fracture criterion (16) was used in the calculations.

$$f^* \geq 0.3. \tag{16}$$

The proposed constitutive equation and damage evolution model include material coefficients whose numerical values for alloys can be estimated using a set of experimental data from independent experiments on the laws of deformation and fracture of alloys in a wide range of deformation rates and temperatures.

The model was used for numerical simulation of tension of flat specimens of titanium and zirconium alloys with strain rates from 0.1 to 1000 s^{-1}.

The initial conditions of specimen's material correspond to the initial uniform temperature field. The numbering of surfaces in the boundary conditions when modeling the tension of flat specimens is shown in Fig.1.

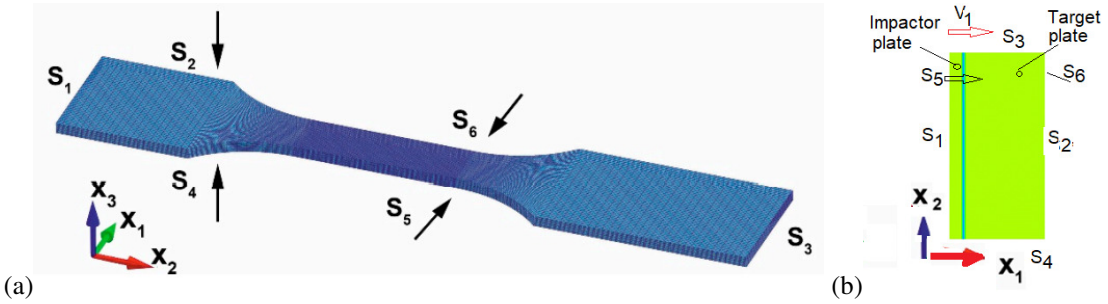

Fig.1. Numbering of surfaces in boundary conditions: (a) uniaxial tension of the flat specimen, (b) plane impact of plates.

Boundary conditions corresponding to uniaxial tension of the specimen (Fig.1a) at a constant strain rate have been used in the form (17):

$$u_{x_2}\big|_{S_1} = 0, u_{x_2}\big|_{S_3} = v_2, u_{x_1}\big|_{S_1} = 0, u_{x_1}\big|_{S_3} = 0, u_{x_3}\big|_{S_1} = 0, u_{x_3}\big|_{S_3} = 0, \sigma_{ij}\big|_{S_2 \cup S_4 \cup S_5 \cup S_6} = 0, \tag{17}$$

where $u_i\big|_{S_j}$ are the components of the particle velocity vector on the surface S_j and v_2 is the tensile velocity.

Boundary conditions corresponding to uniaxial tension of the specimen (Fig.1b) at a constant strain rate have been used in the form (18):

$$\sigma_{11}\big|_{S_1} = 0, \sigma_{11}\big|_{S_2} = 0, \sigma_{22}\big|_{S_3} = 0, \sigma_{22}\big|_{S_4} = 0, \sigma_{33}\big|_{S_5} = 0, \sigma_{33}\big|_{S_6} = 0, \tag{18}$$

where σ_{ij} are the components of the stress tensor on the surface S_k.

The computer simulations were performed with the use of LS DYNA (ANSYS WB 15.2, ANSYS, Inc., Canonsburg, PA, USA) software. The calculations were carried out using the finite-difference scheme of second order accuracy. Computational domains were meshed with eight-node linear bricks and reduced integration together with hourglass control.

3. Results and discussion

Numerical simulations of titanium alloy specimens subjected to tension were out carried to study damage kinetics and the influence of damage on mechanical behavior. The calculated values of effective plastic strain obtained in the simulation uniaxial high-rate tension of Ti-5Al-2.5Sn samples in comparison with experimental data [14] are shown in Fig.2. Two inclined stationary shear bands were formed in the neck zone. The simulations demonstrate the important role of

plastic strain localization phenomena in dynamic damaging processes of HCP alloys. The cracks position indicates a very strong correlation between the plastic strain localization and damage accumulation. The evolution of the calculated strain field and the fracture zone configuration are consistent with the data obtained by the digital image correlation (DIC) method at strain rates from 0.1 to 1000 s^{-1}. The value of the plastic deformation of the beginning of the formation of mesoscopic shear bands at different loading conditions correlates with values estimated by the Considère criterion (19) [16].

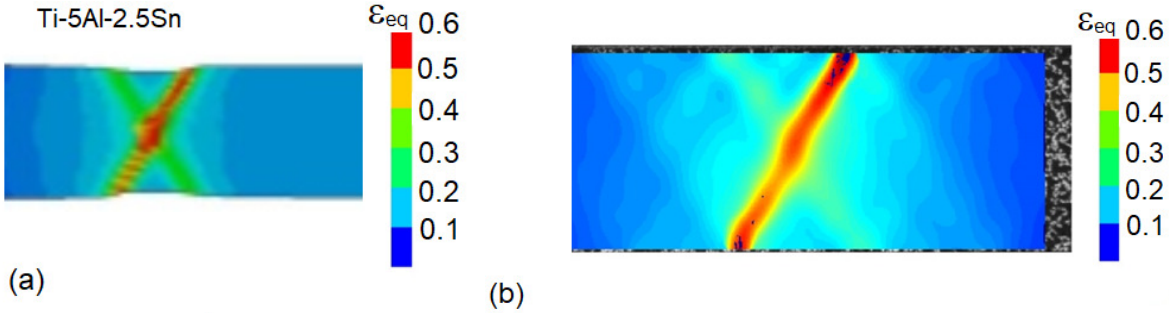

Fig.2 (a) Calculated equivalent strain in gage zone of flat specimen of Ti-5Al-2.5Sn under tension at 1000 s^{-1} before crack formation; (b) the experimental data [14] on strain distribution determined by the DIC method.

$$\sigma_s = \frac{d\sigma_s\left(\varepsilon^p_{eq}, \dot{\varepsilon}^p_{eq}, T\right)}{d\varepsilon^p_{eq}}. \tag{19}$$

The computational stress-strain diagrams obtained when simulating uniaxial high-rate tension of Ti-5Al-2.5Sn, α-Zr alloy samples in comparison with experimental data are shown in Fig.3. The calculated value of the strain A_{ist} α-Zr at the beginning of the formation of a stationary strain localization band is shown in Fig.3b.

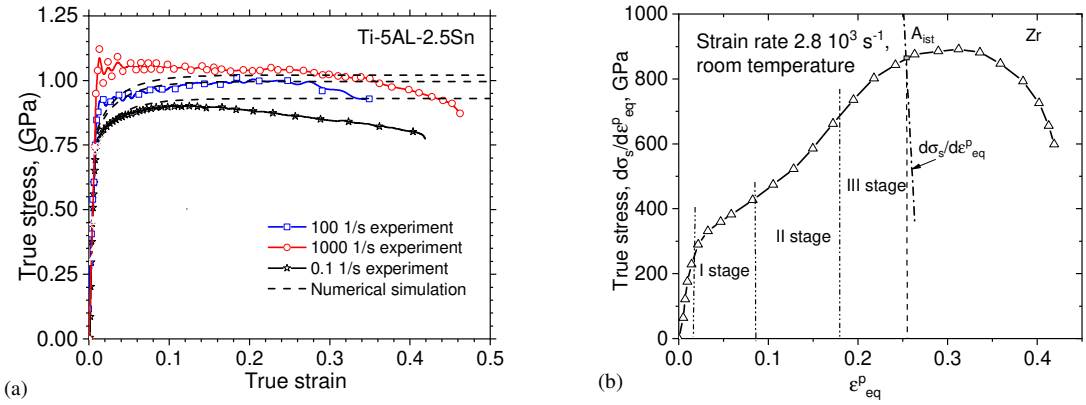

Fig.3. (a) Calculated stress versus strain and experimental true stress vs true strain curves of Ti-5Al-2.5Sn [14]; (b) calculated true stress vs true strain curves and strain hardening of α-Zr under tension.

The processes of spall fracture of Ti-5Al-2.5Sn under sub microsecond shock pulse loading were investigated by the method of numerical simulation. The calculated free surface velocity profile of the 4 mm thick plate (Ti-5Al-2.5Sn) subjected to planar impact (660 m/s) by 2 mm aluminum plate closely matches experimental data, as seen in Fig.4a [17]. The calculated free surface velocity profile of the 5 mm thick plate (α-Zr) subjected to planar impact (600 m/s) by 2.5 mm aluminum 6082-T6 plate closely matches experimental data, as seen in Fig.4b [18]. The spall

fracture is a result the damage nucleation, growth and coalescence under repeated processes tension and compression conditions in interacted waves.

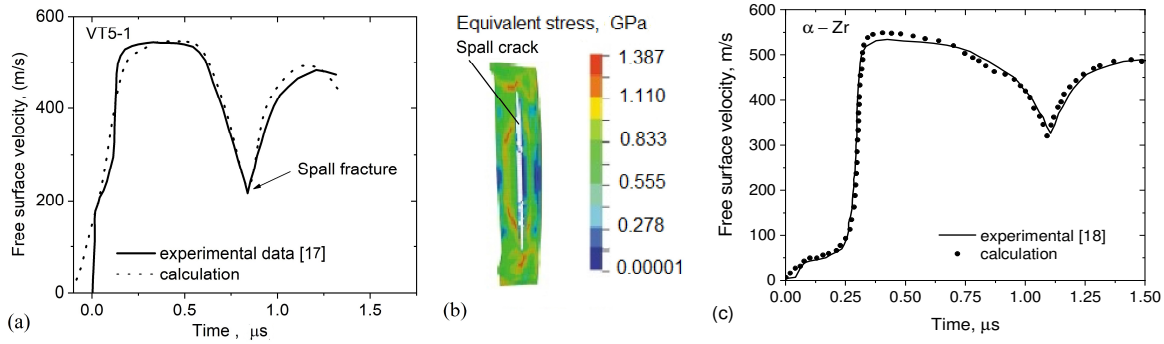

Fig.4. (a) Shock wave profiles in Ti-5Al-2.5Sn; solid curve is the experimental data [17], dashed curve is calculated data; (b) the distribution of the equivalent stress near spall crack at it's formation of in the Ti-5Al-2.5Sn; (c) shock wave profiles in Zr (b); solid curve is the experimental data [18], the calculated data is shown by dashed curve.

Shock pulses of the amplitude up to 6 GPa (or particle velocity amplitude up to 290 m/s) propagate in the Ti-5Al-2.5Sn plate with a formation of the two-wave structure of the shock wave. The elastic precursor wave velocity derived from simulation (6.148 km/s) is in agreement with experimental data (~6.15 km/s). The bulk wave velocity depends on the load amplitude due to plastic deformation occurring in its front. The numerical experiments have shown that the bulk wave velocity approaches 5.1 km/s under considered pulse-load amplitudes. Release waves are formed due to the reflection of the shock wave from free surfaces. Interaction of opposite release waves results in the negative pressure sufficient to the spall crack nucleation. Reflection of release wave from the spall crack surface results in the reloading wave formation. The free surface velocity growth occurs due to reloading wave arrives at the free surface, as seen in Fig.4a. The distribution of local values of the flow stress σ_{eq} in the spallation zone changes in time. Note, the stress triaxiality parameter $\eta = -p/\sigma_{eq}$ is changed in zone of spall crack formation. The stress relaxation is caused by the development of inelastic deformation in the condensed phases of the alloy and the formation of free surfaces in meso- and macroscale voids. The spall crack is shown in Fig.4b are formed by coalescence of damaged mesoscopic volumes. In the spallation zone there are local volumes in which the alloy has undergone large plastic deformation during the spallation. These inelastic deformations arise upon repeated loading of the alloy by reflected loading and unloading waves. Therefore the surfaces of spall macro crack in HCP alloys have a relief. The specificity of the mechanical behavior of considered first isomechanical subgroup HCP alloys is that the contributions to the flow stress from dislocation slip and twinning at temperatures near to room temperature and pressures less ~4 GPa are comparable. However, the ratio of these contributions changes significantly at the localization of plastic flow, and changing the loading from tensile to compressive. In the proposed model, change in the contributions of twinning to the flow stress is described by relations (12) and (13). The use of relation (14) is necessary to adequately take into account the change in the contribution of damage evolution when changing from tensile to compressive loads. The introduction of the damage contribution into the model made it possible to obtain a qualitatively correct and good quantitative description of the unloading and reloading wave profiles in the calculation.

4. Conclusion

The regularities of mechanical behaviour of HCP metals and alloys (α-Ti, α-Zr) belonging to the first isomechanical subgroup are similar. The constitutive equation for describing the

elastoplastic behavior of HCP alloys with c/a < 1.633 is constructed within the framework of modern physical concepts of the main mechanisms providing plastic flow including the generation and sliding of dislocations, twinning and de-twinning.

The proposed constitutive equations and damage model make it possible to describe the main regularities of the mechanical behavior of a subgroup of HCP alloys with a lattice parameter ratio c/a < 1.633 in a wide range of strain rates and weak shock wave amplitudes.

The introduction of the twinning contribution into the model made it possible to obtain a qualitatively correct and good quantitative description of the unloading and reloading wave profiles in the calculation.

The mathematical form of constitutive equation differs from the equations for BCC and FCC materials.

The fracture of alloys belonging to the isomechanical subgroup of HCP metals with a ratio of the crystal lattice parameters c/a <1.633 is ductile under tension with strain rates from 100 to 1000 s^{-1}. The results of experimental studies and numerical simulations have shown that the cracks formation during dynamic fracture of HCP titanium and zirconium alloys under tension occurs near localized shear bands.

The dynamic fracture of alpha titanium and zirconium alloys under tension at strain rates from 100 to 10^3 s^{-1} is a result of nucleation, growth and coalescence of damages in localized bands of plastic deformation.

The obtained results of numerical simulation of the spall fracture of alpha titanium and zirconium alloys are consistent with the available experimental data on plane impact of plates. It is shown that spall microcracks oriented perpendiculars to the direction of impact are formed by coalescence of damaged mesoscopic volumes. In the spallation zone there are local volumes in which the alloys have undergone large plastic deformation in the process of spall fracture. These inelastic deformations arise upon repeated loading of the alloy by reflected loading and unloading waves.

Acknowledgement

This work was financially supported in part by the Russian Science Foundation (project No. 22-79-00162) and the Tomsk State University Project (НУ 2.4.7.22 ИГ).

5. References

[1] Follansbee P.S., *Fundamentals of Strength. Principles, Experiments, and Applications of an Internal State Variable Constitutive Formulation*. (New Jersey: TMS-Wiley, 2014); doi: 10.1002/9781118808412

[2] Boyer R., Collings E.W., Welsch G., *Materials properties handbook: Titanium alloys.* (ASM International, 1994).

[3] Armstrong R.W., Zerilli F.J., *Proc. ASME Mater. Div*., MD69-1, 417, 1995.

[4] Gao C.Y., Zhang L.C., Yan H. X., *Materials Science and Engineering* – A, **528**, 4445, 2011; doi:10.1016/j.msea.2011.02.053

[5] Nemat-Nasser S., Guo W.G, Cheng J.Y., *Acta Mater.* **47**, 3705, 1999; doi: 10.1016/S1359-6454(99)00203-7

[6] Song Y., Voyiadjis G.Z., *European Journal of Mechanics* – A, *Solids*, **83**, 104034, 2020; doi: 10.1016/j.euromechsol.2020.104034

[7] Frost H.J., Ashby M.F., *Deformation-mechanism maps: the plasticity and creep of metals and ceramics*. (Pergamon Press: Oxford, UK, 166, 1982).

[8] Chernyaeva T.P., Gritsina V.M., *Voprosy Atomnoj Nauki i Tekhniki*, **2**(92), 15, 2008.

[9] Skripnyak V.V., Skripnyak V.A., *Journal of Applied Physi*cs, **131**, 165902, 2022; doi: 10.1063/5.0085338
[10] Kerley G.I., *Equations of state for titanium and Ti6A14V alloy:Report.,* Albuquerque, **3785**, 35, 2003; doi: 10.2172/918300
[11] Steinberg D.J., Cochran S.G., Guinan M.W., *Journal of Applied Physics*, **51**(3), 1498, 1980; doi: 10.1063/1.327799
[12] Neilsen K.L., Tvergaard V., *Eng. Fract. Mech*., **77**, 1031, 2010; doi: 10.1016/j.engfracmech.2010.02.031
[13] Skripnyak V.V., Kozulyn A.A., Skripnyak V.A., *Mater Phys. Mech.,* **42**, 415, 2019; doi: 10.18720/MPM.4242019_6
[14] Skripnyak V.V., Skripnyak E.G., Skripnyak V.A., *Metals,* **10**(3) 305, 2020; doi: 10.3390/met10030305
[15] Bai Y., Wierzbicki T., *International Journal of Plasticity*, **24**, 1071, 2008; doi: 10.1016/j.ijplas.2007.09.004
[16] Yasnikov I.S., Vinogradov A., Estrin Y., *Scripta Materialia*, **76**, 37, 2014; doi: 10.1016/j.scriptamat.2013.12.009
[17] Razorenov S.V., Utkin A.V., Kanel' G.I., Fortov V.E., Yarunichev A.S., Baumung K., Karow H.U., *High Pressure Res*., **13**(6), 367, 1995; doi: 10.1080/08957959508202588
[18] Hazell P.J., Appleby-Thomas G.J., Wielewski E., Escobedo J.P., *Philosophical Transactions of the Royal Society A: Mathematical, Physical and Engineering Sciences*, **372,** 20130204, 2014; doi: 10.1098/rsta.2013.0204